ACS APPLIED MATERIALS & INTERFACES

Research Article

www.acsami.org

Synthesis of Natural Cellulose-Templated TiO_2/Ag Nanosponge Composites and Photocatalytic Properties

Dong-Hui, Yu,[†] Xiaodan, Yu,*[,†] Changhua, Wang,[‡] Xian-Chun, Liu,[†] and Yan, Xing*[,†]

[†]Faculty of Chemistry, Northeast Normal University, Changchun 130024, People's Republic of China

[‡]College of Chemistry and Biology, Beihua University, Jilin 132013, People's Republic of China

Supporting Information

ABSTRACT: In this paper, TiO_2/Ag sponge-like nanostructure composites have been prepared by the surface sol–gel method with the template of natural cellulose, which is relatively simple, low-cost, and environmentally friendly. The Ag nanoparticles are deposited on the TiO_2 nanosponges through UV irradiation photoreduction of silver nitrate solutions. The physicochemical properties of as-prepared composites are characterized by XRD, BET, SEM, TEM, XPS and UV–vis DRS techniques. The UV-light photocatalytic activities of the composites are evaluated through the photodegradation of two model organic molecules including RhB and salicylic acid. The experimental results show that the photocatalytic activities of TiO_2/Ag nanosponge composites are superior to that of P25, pure TiO_2 nanoparticle aggregates synthesized by the hydrothermal method and pure TiO_2 nanosponge. The superior activities of TiO_2/Ag nanosponge composite photocatalysts can be attributed to the unique nanosponge morphology, uniform dispersion of Ag nanoparticles, and strong interaction between Ag and TiO_2 nanosponges.

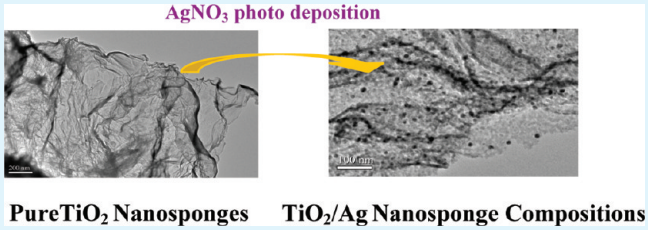

KEYWORDS: *natural cellulose, nanosponge, sol–gel, photoreduction, photocatalysis*

1. INTRODUCTION

Recently, the micro/nanostructural semiconductor metal oxides with a porous structure have been significant interest for the catalyst, filter, photocatalyst, battery and sensor applications.[1−4] Many of these applications require the extensive gas/solid or fluid/solid contact which can provide the porous architectures. For photocatalysts, porous materials are attractive since the porosity minimizes the distance between the site of photon absorption and electron/hole redox reactions so as to enhance the efficiency.[5−7] Therefore, many strategies have been developed to prepare the porous photocatalysts with the high surface area, tunable distribution of pore size and controllable morphology. Up to now, many interesting textural materials have been synthesized for the photocatalytic degradation of organic pollutants, such as nanofibers, nanotubes, nanosponges, spheres, etc.[8−10] Although much efforts have been devoted to the synthesis of porous photocatalysts, there are still many barriers to the targeted products. On one hand, controlling over both the pore wall composition and the morphology is difficult, and the calcination of precursor materials often leads to a dense and fully collapsed structure because of the thermal instability of inorganic network during crystallization. On the other hand, the sophisticated synthetic schemes are usually employed, and the synthetic conditions are rather restrictive (e.g., ordered mesoporous structure synthesized by using the block copolymer as template or macroporous structure synthesized by using the latex sphere as template[11−13]). From the perspective trend of application, the fabrication of porous photocatalysts via a low cost and simple method is still a challenge. Therefore, the facile approaches for the preparation of micro/nano structural photocatalysts with the favorable morphology and porous structure are highly demanded.[14−17]

Besides the efficient control over the structural properties of photocatalyst themselves, the fabrication of metal-semiconductor oxide composites (e.g., TiO_2/Ag,[18] ZnO/Au,[19] WO_3/Pt[20]) is another very dynamic research area to improve the photocatalytic activities of semiconductor oxide photocatalysts. The electron transfer from semiconductor oxides to metal nanoparticles can occur, which can decrease the number of electron/hole recombination events and improve the photocatalytic performance of semiconductor oxide-based catalysts. Because the porosity can enhance the diffusion of pollutant throughout the photocatalyst channels and the metal particles act as electron sinks, the recombination of photon-generated electron/hole pairs within the semiconductor oxides can be decreased. It is expected that the high photocatalytic efficiencies of semiconductor oxides will be achieved by the controlled porosity and addition of metal sites.

In the present work, we demonstrate an efficient and facile approach for the synthesis of TiO_2/Ag nanosponge materials using the biological template-cellulose fibers (filter paper) associated with the surface sol–gel process.[21] The natural cellulose fibers, which can be easily available, possess surface hydroxyl groups and provide a suitable vehicle for the surface

Received: March 12, 2012
Accepted: May 1, 2012
Published: May 1, 2012

sol−gel process. The experimental results show that the as-adopted method is flexible to faithfully replicate the morphological hierarchies of natural cellulosic substances from macroscopic to nanometer scales.[22] The Ag nanoparticles are deposited on the TiO_2 nanosponges through UV irradiation photoreduction of silver nitrate solutions. The UV-light photocatalytic activities of the composites are evaluated through the photodegradation of two model organic molecules including RhB and salicylic acid.

2. EXPERIMENTAL SECTION

2.1. Preparation of TiO_2 Nanosponge. In a typical procedure, six piece of commercial filter paper was placed in a suction filtering unit and washed by ethanol, followed by drying with air flow. Three milliliters of Titanium tetraisopropoxide (TTIP, 98%) was added to 20 mL of isopropy alcohol with stirring. The pH value of the solution was adjusted to 1−2 by 36−38% HCl solution. In another container, 0.3 mL of deionized water was added to 5 mL of isopropy alcohol under stirring. The above two solutions were added dropwise into the filter paper alternatively. After that 40 mL of ethanol was then immediately filtered to remove the unreacted metal alkoxide. Then the filter papers were dried with airflow. By the process of filtration/deposition, thin titania gel layers were deposited on the morphologically complex surface of paper. Finally, the resultant paper/titania composites were calcined in air at 723 K for 6 h to remove the original filter paper. For comparison, the same sol obtained was hydrothermal treated at 200 °C for 2 h to obtain TiO_2 nanoparticles.

2.2. Preparation of Ag/TiO_2 Nanosponge. One-tenth of a gram of prepared TiO_2 nanosponge materials was added into 15 mL of deionized water, and a certain amount of $AgNO_3$ solution was dissolved in the above mixture. Then the mixture was irradiated under UV lights (intensity 4 mW/m^3) for 60 min to reduce silver nitrate. The resulted deposition with gray color was washed three times with distilled water and absolute ethanol respectively to remove the residual silver ions and unreacted silver nitrate and finally thermal treatment at 723 K, which was denoted as TiO_2/Ag-x, where x was the Ag loading content (wt %) in the products. Elemental analysis for the Ag loading content of in the products were 1.1, 3.2, 5.1, and 8.3%, respectively by ICP-AES were as expected.

2.3. Characterization. Elemental analysis was performed on a Leeman Prodigy Spec ICP-AES. X-ray diffraction (XRD) patterns of Ag/TiO_2 samples (2θ ranges from 10 to 70°) were recorded at room temperature with a scanning speed of 2° min^{-1} using Cu K α radiation (λ=0.154 nm) from a 40 kV X-ray source (Bruker D8 Advance) and a diffracted beam monochromator operated at 40 mA. The textural structures were measured by N_2 adsorption at 77 K with a Micromeritics TriStar ASAP 3000 system. The specific surface areas of Ag/TiO_2 samples were measured using the Brunauer−Emmett−Teller (BET) method. Field-emission Scanning Electron Microscope (FE-SEM) was obtained using an XL30 ESEM-FEG microscope (FEI Co.). Transmission electron micrographs (TEM) were obtained using a JEOL-2011F microscope operating at an accelerating voltage of 200 kV. X-ray photoelectron spectroscopy (XPS) measurements were performed on a PHI 5000C ESCA system with Mg KR source operated at 14.0 kVand 25 mA. All the binding energies were referenced to the C1s peak at 284.6 eV from the surface adventitious carbon.

2.4. Photocatalytic Test. The photoreactor was designed with an internal light source (125W high pressure mercury lamp with main emission wavelength 313 nm) surrounded by a quartz jacket, where the suspension including the solid catalyst (0.10 g) and an aqueous RhB/salicylic acid (90 mL, 25 mg/L) completely surrounded the light source. The suspension was ultrasonicated for 10 min and stirred in the dark for 30 min to obtain a good dispersion and to establish the adsorption−desorption equilibrium between the organic molecules and the catalyst surface. The temperature of the suspension was maintained at 30 ± 2 °C by circulation water through an external cooling coil, and the system was open to air. Decreases in the concentrations of dyes were analyzed by (Shimadzu, UV-2450) UV−vis−NIR spectrophotometer at λ = 553 nm for RB and λ = 348 nm for salicylic acid, respectively. At given intervals of illumination, the samples of the reaction solution were taken out, and then centrifuged and filtrated. Finally, the filtrates were analyzed. To investigate the stability of the catalysts, the photocatalytic reaction for each sample was carried out three times.

3. RESULTS AND DISCUSSION

3.1. Preparation. In the previous reports, the TiO_2 nanosponges with porous structure were synthesized by sol−gel with hydrothermal and surfactant template, etc.[23−25] To the best of our knowledge, there is no report of using the natural cellulosic substances as template to prepare TiO_2 sponge-like nano materials. In the present studies, we take advantage of the surface sol−gel process to faithfully replicate the morphological hierarchies of natural cellulosic substances from macroscopic to nanometer scales. The surface sol−gel process can be explained as that a solid substrate with the hydroxyl groups on its surface is allowed to react with the metal alkoxides in solution to form covalently bound surface monolayers of the metal alkoxides and subsequent hydrolysis to give nanometer-thin oxide layers. The natural cellulose fibers possess hydroxyl groups on the surface, and provide a suitable vehicle for the surface sol−gel process. We attempt to use TTIP as a precursor to achieve the sol−gel process. The formation of cellulosic fiber paper covered by the titania sol is illustrated in Scheme 1. First of all, the two

Scheme 1. Schematic Illustration of the Synthetic Process for TiO_2/Ag Nanosponge Materials[a]

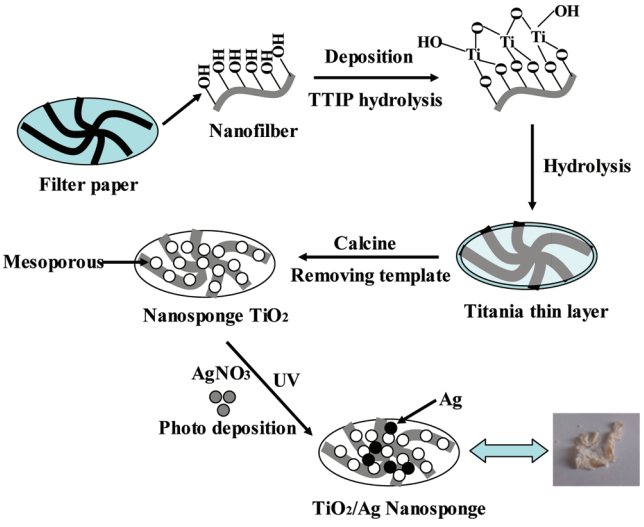

[a]TTIP, titanium tetraisopropoxide.

solutions (TTIP + isopropy alcohol and water + isopropy alcohol) are added dropwise into the filter paper alternatively; Second, the one layer of titania is deposited on the morphologically complex surface of filter paper; Third the resultant paper/titania composites are calcined to remove the original filter paper and the TiO_2 nanosponge materials can be obtained; Finally, the Ag nanoparticles are deposited on the TiO_2 nanosponges through photoreduction of the silver nitrate solutions under UV irradiation.

3.2. Photocatalyst Characterizations. To investigate the morphology of TiO_2/Ag nanosponge materials and distribution of the silver nanoparticles, the pure TiO_2 nanosponge and Ag/

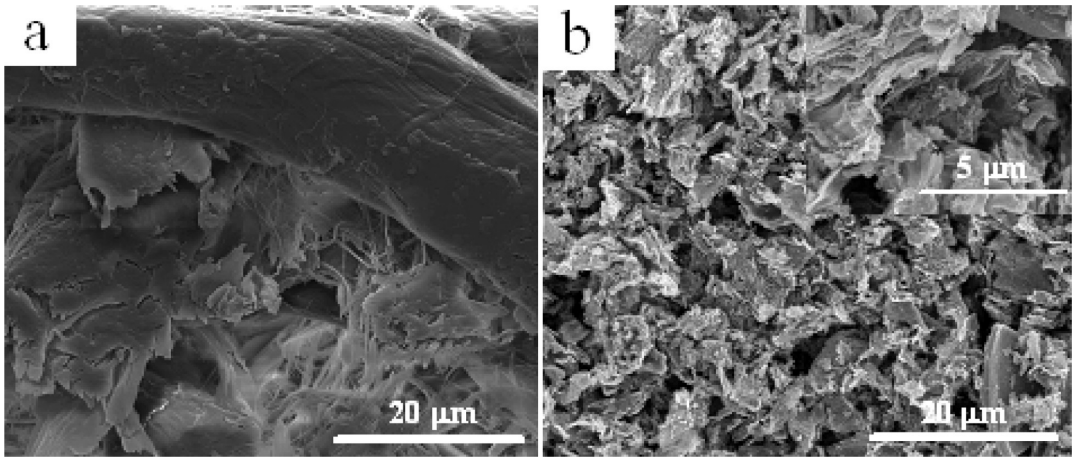

Figure 1. SEM image of (a) filter paper and (b) TiO_2/Ag-3.2% nanosponge materials.

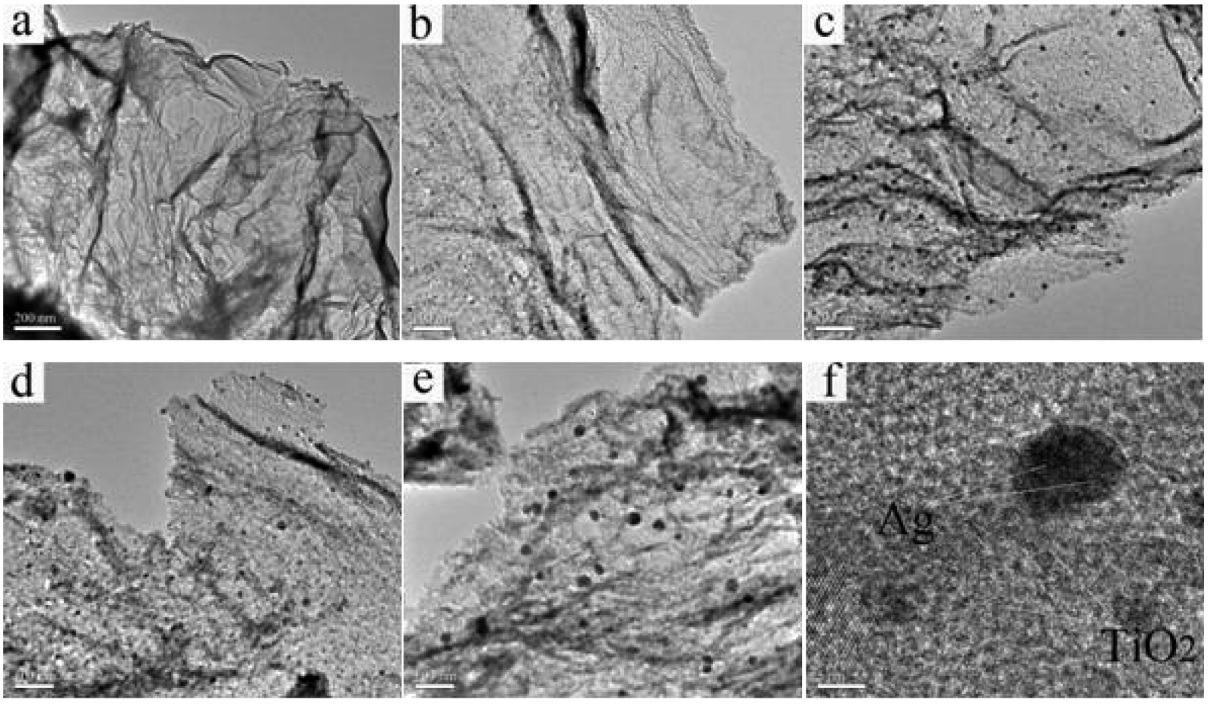

Figure 2. TEM images of (a) pure TiO_2, (b) TiO_2/Ag-1.1%, (c) TiO_2/Ag-3.2%, (d) TiO_2/Ag-5.1%, (e) TiO_2/Ag-8.3%, and (f) HRTEM image of TiO_2/Ag-5.1%.

TiO_2 composites with different loading contents are examined by SEM and TEM. Figure 1a shows the SEM image of the filter template. It can be observed that the adopted filter template is composed of fibers and display a multilayered structure. After the sol−gel and calcinations process, the original morphology of the filter template can be well-maintained. As shown in Figure 1b, the resulting materials display multilayered structure and the surface is coarse. Additionally, Ag nanoparticles are hardly observed because of their small size.

Figure 2 shows the TEM images of pure TiO_2 and TiO_2/Ag nanosponge composites with different Ag loading contents. By Figure 2a, the sample is mainly composed of two-dimensional membrane features with thickness uniformity. The appearance of membrane feature may be generated by the exfoliation from multilayered aggregates. Obviously, the porosity and two-dimensional membrane features give them the sponge-like appearance. Figure 2b−e shows the TEM images of TiO_2/Ag nanosponge composites with different Ag loading contents. It is clearly shown that the Ag nanoparticles are well dispersed on the TiO_2 thin layer without aggregation. Furthermore, with the increasing of Ag loading content, the sizes of Ag particles become larger, which are presented in Figure 3. The particle size distribution of silvers is in the range from 4.2 to 23.8 nm by the TEM images analysis. To further obtain more structural information on TiO_2 nanosponges and Ag nanoparticles, we performed HRTEM. As shown in Figure 2f, the estimated interplanar spacing of TiO_2 nanosponge and Ag nanoparticles is 0.35 and 0.24 nm, which corresponds to the (101) and (111) plane of anatase TiO_2 and cubic Ag, respectively.

The crystalline phases of the TiO_2/Ag nanosponge composites with different Ag loading contents are characterized by XRD measurements. For comparison, as-prepared pure TiO_2 nanosponge is also tested. As shown in Figure 4, both pure TiO_2 and TiO_2/Ag nanosponge composites with different

dx.doi.org/10.1021/am3004363 | ACS Appl. Mater. Interfaces 2012, 4, 2781−2787

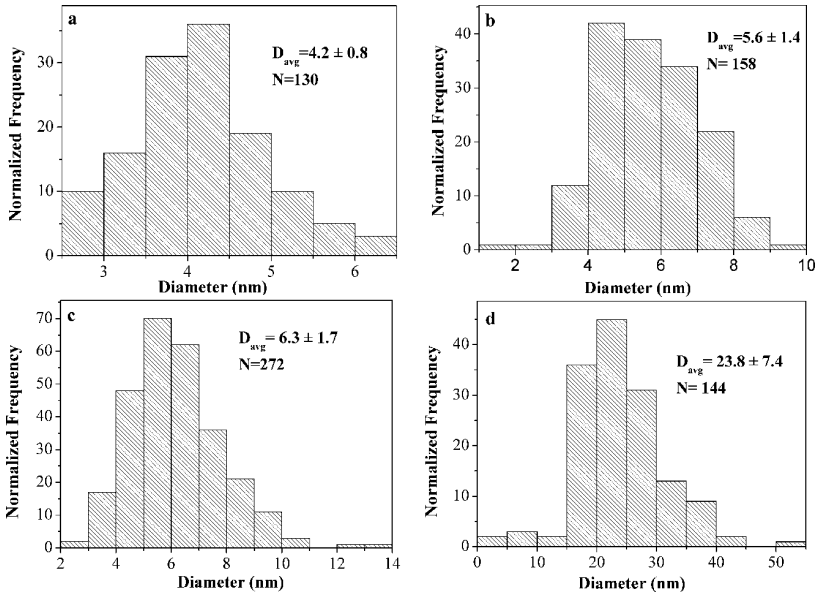

Figure 3. Ag size distributions corresponding to (a) TiO_2/Ag-1.1%, (b) TiO_2/Ag-3.2%, (c) TiO_2/Ag-5.1%, and (d) TiO_2/Ag-8.3%.

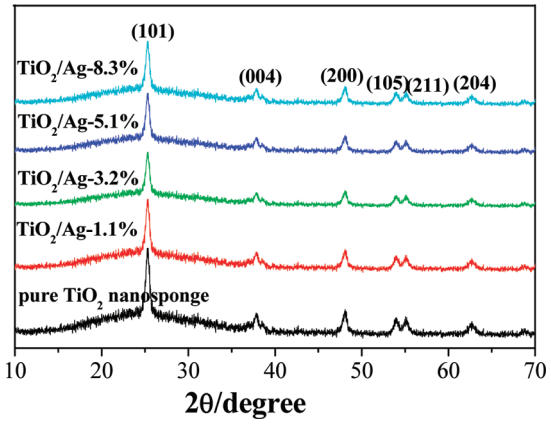

Figure 4. XRD patterns of as-prepared TiO_2/Ag (1.1%, 3.2%, 5.1%, and 8.3%) and pure TiO_2 nanosponge materials.

Ag loading contents exhibit the uniform anatase structure with characteristic 2θ values at (25.31, 37.90, 48.02, 53.92, 55.10, and 62.83°), respectively (JCPDS No. 21−1272). The diffraction peaks originated from Ag are hardly detected in the TiO_2/Ag samples. In addition, there is no remarkable shift of all diffraction peaks implying that no TiO_2-nAg_xO is formed in all of the as-prepared samples.[26] This may be due to the facts of: (i) The dispersion of Ag particles are homogeneous on the surface of product; (ii) The peaks of metallic Ag is difficult to be detected because of low Ag loading content; or (iii) the most intense of Ag peaks is overlapped by those of TiO_2.

The chemical states of Ag species in the TiO_2/Ag nanosponge compositions are examined by the XPS measurement. The banding energies in the XPS spectra presented in Figures 5 and 6 are calibrated by contaminatant carbon (C1s = 284.6 eV). The full XPS spectrum from TiO_2/Ag-3.2% sample is shown in Figure 5a. Three sets of major peaks can be assigned to O1s, Ti2p and Ag3d. Among them, the binding energies of Ti $2p_{3/2}$ and O1s are 458.9 and 529.7 eV respectively, which are consistent with the values of TiO_2.[27] Figure 5b shows the XPS of the Ag $3d_{5/2}$ and Ag $3d_{3/2}$ binding energy regions. The determined binding energies of Ag $3d_{5/2}$ and Ag $3d_{3/2}$ are 367.7 and 373.7 eV respectively, and the spin energy separation is 6.0 eV. This is the characteristic of metallic silver (Ag^0).[28] The signals of Ag in TiO_2/Ag samples with different surface Ag contents are shown in Figure 6a. With the surface Ag content in TiO_2/Ag samples increasing, the Ag $3d_{5/2}$ and $3d_{3/2}$ binding energies have largely negative shifts

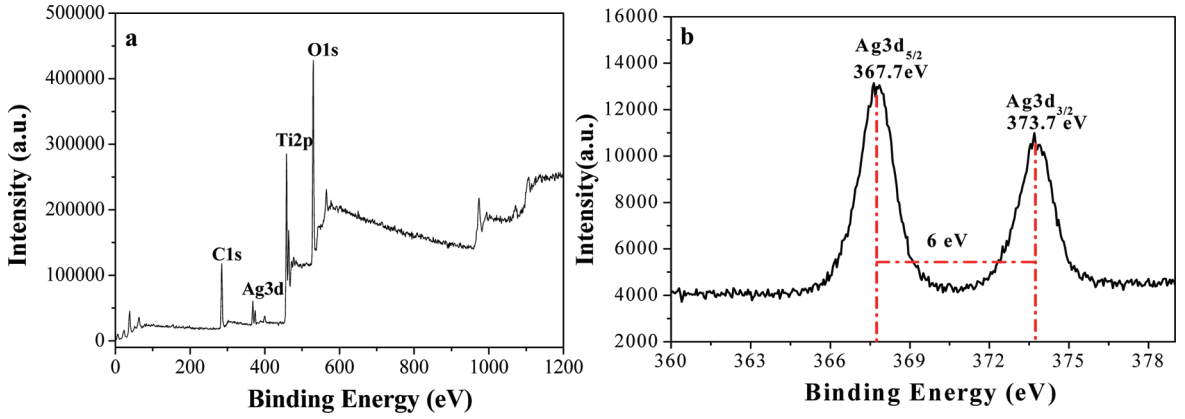

Figure 5. (a) XPS survey scan of the TiO_2/Ag-3.2%; (b) Ag 3d XPS spectra of TiO_2/Ag-3.2%.

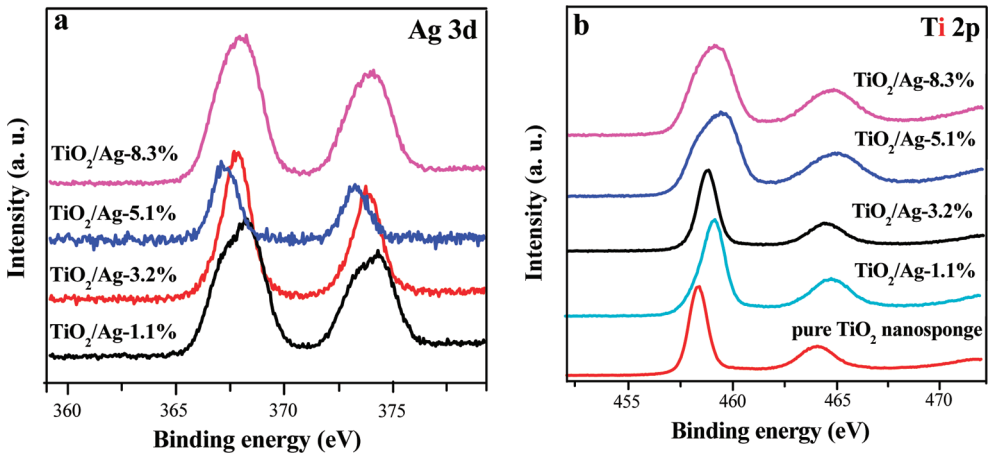

Figure 6. (a) Ag 3d and (b) Ti 2p XPS spectra of different TiO_2/Ag nanosponge composites.

compared to those of bulk Ag (368.3 eV for $3d_{5/2}$ and 374.3 eV for $3d_{3/2}$).[28] It is indicated that some electrons may transfer from TiO_2 to metallic Ag, and there is a strong interaction between Ag particles and TiO_2 support. To obtain further evidence about the interaction between the Ag nanoparticles and TiO_2, the Ti chemical states are also examined by the XPS (Figure 6b), and the results are described below. With the surface Ag content in TiO_2 nanosponges increasing, the Ti $2p_{3/2}$ binding energy band shifts to a higher position than that of pure TiO_2, which indicates a lower electron density of the Ti atoms in the TiO_2/Ag materials. From Figure 6a and 6b, it can be seen that the peaks of Ag 3d and Ti 2p of all TiO_2/Ag samples shift reversely, which suggests that the metallic Ag and TiO_2 has a strong interaction in TiO_2/Ag nanosponge composites. The interaction between the metallic Ag and TiO_2 in the Ag/TiO_2 nanosponge composties can effectively inhibit the recombination of excited electrons and holes, because the Ag particles on the surface of TiO_2 will act as electron acceptors and give favor to separate the photoexcited electron–hole pairs. Furthermore, among the TiO_2/Ag samples, the TiO_2/Ag-5.1% sample exhibits the largest shifts both in Ag 3d and Ti 2p peaks, which suggests the strongest interaction between the metallic Ag and TiO_2. However, when the surface Ag content of TiO_2/Ag samples exceeds 5.1%, the excessive Ag particles will also act as the trapping sites through accepting the photoexcited electrons from the TiO_2 valence band, which decreases the number of photoinduced electrons and the activities of photocatalysts accordingly.

Figure 7 shows nitrogen adsorption–desorption isotherms and pore size distribution curves of TiO_2/Ag nanosponges with different Ag loading contents and the pure TiO_2 nanosponge for comparison. Both TiO_2/Ag nanosponge composites exhibit a type IV adsorption isotherm with a H3 hysteresis loop according to BDDT classification, which are typical characteristics of mesoporous materials.[29] The surface textural properties of all the as-prepared TiO_2 nanocomposite samples are summarized in Table 1. The above results obviously show that the BET surface area is strongly dependent on the Ag loading content. It can be seen from Table 1 that the BET surface area increases with the Ag loading content to reach the maximum at TiO_2/Ag-5.1%, and then decreases for larger Ag loading content. At TiO_2/Ag-8.3% the BET surface area reaches the minimum because of sintering of the smaller particles into the bigger particles.

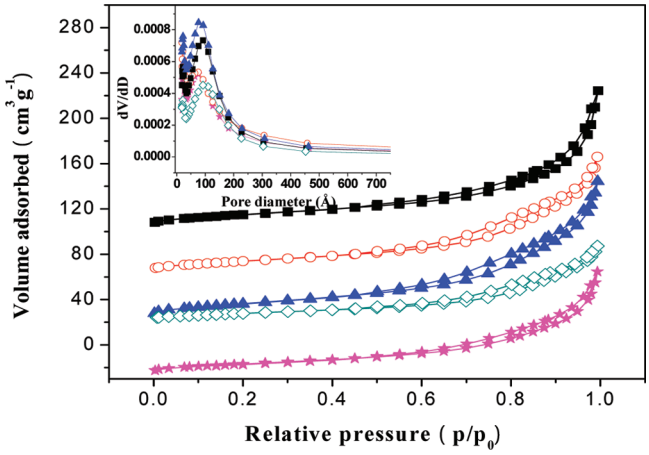

Figure 7. Nitrogen adsorption–desorption isotherms and pore size distribution profiles (insert) according to BJH desorption dV/dD pore volume of as-prepared composites. (○) TiO_2/Ag-1.1%; (■) TiO_2/Ag-3.2%; (▲) TiO_2/Ag-5.1%; (◊) TiO_2/Ag-8.3%; (★) pure TiO_2 nanosponge.

Table 1. Textural Parameters of As-Prepared Samples

samples	pure TiO_2 nanosponge	TiO_2/Ag (1.1%)	TiO_2/Ag (3.2%)	TiO_2/Ag (5.1%)	TiO_2/Ag (8.3%)
S_{BET}[a] (m^2/g)	44.954	53.235	53.852	65.234	35.701
D_p[b] (Å)	76.2	64.4	92.7	76.8	92.1
V_p[c] (cm^3/g)	0.121	0.169	0.130	0.162	0.085

[a]BET surface area, which is calculated using. [b]Median pore diameter, which is calculated using the BJH model based on nitrogen absorption isotherm. [c]Pore volume.

3.3. Photocatalysis Studies. The dye RhB and salicylic acid are selected as the model molecules to evaluate the UV-light photocatalytic properties of as-prepared TiO_2/Ag nanosponge composites. The pure TiO_2 nanosponge, TiO_2 powder and P25 are also tested for comparison. The present photocatalytic tests are carried out in an aqueous solution containing oxygen (dissolved in the reaction system from air). In the current photocatalytic system, the direct photocatalysis of RhB is hardly observed after UV-light irradiation for 60 min in the absence of photocatalyst. The results in Figure 8a show that the photocatalytic activities of five catalysts toward the

dx.doi.org/10.1021/am3004363 | ACS Appl. Mater. Interfaces 2012, 4, 2781–2787

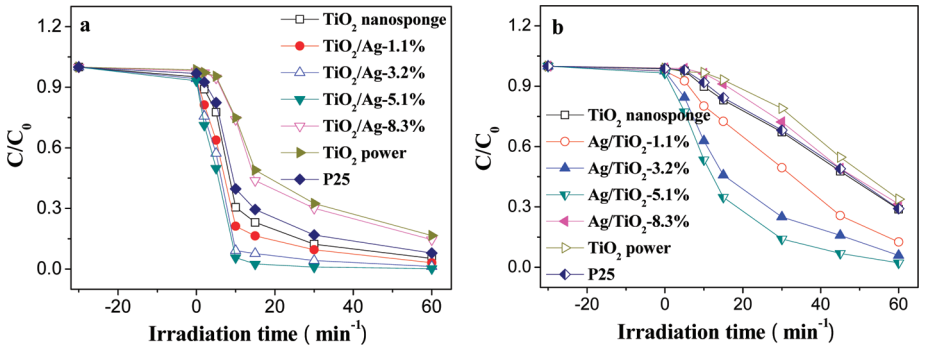

Figure 8. Photocatalytic degradation of (a) the aqueous RhB (25 mg/L, 90 mL) and (b) the aqueous salicylic acid with as-prepared TiO_2/Ag (1.1, 3.2, 5.1, and 8.3%), pure TiO_2 nanosponge, P25 and TiO_2 powder.

degradation of RhB. The photocatalytic activity is in the order of TiO_2/Ag-5.1% > TiO_2/Ag-3.2% > TiO_2/Ag-1.1% > pure TiO_2 nanosponge > P25 > TiO_2/Ag-8.3% > TiO_2 powder. These results indicate that (i) the TiO_2/Ag nanomaterials with nanosponge structure exhibit higher photocatalytic activities than the pure TiO_2 powder; (ii) the activity of TiO_2/Ag system monotonically increase with the increasing of Ag loading content from 1.1 to 5.1%, whereas the activity sharply decrease as the Ag loading content reach 8.3%; (iii) the TiO_2/Ag system show higher photocatalytic activity than that of the pure TiO_2 nanosponge and P25 except TiO_2/Ag-8.3%.

The photocatalytic activities of TiO_2/Ag system are further studied by degradating salicylic acid under UV-light irradiation. All the experimental conditions are the same as those of 4-NP degradation, and the results are shown in Figure 8b. In the current photocatalytic system, the degradation of salicylic acid (100 mg L^{-1}) by direct photolysis is hardly observed after UV-light irradiation for 60 min. However, the degradation of salicylic acid reach to 97.8% after 60 min UV-light irradiation in the presence of TiO_2/Ag-5.1%. Under the same conditions, the degradation of salicylic acid reach to 87.5, 94.2, 66.2, 71.2, 70.9, and 60.6%, respectively, with TiO_2/Ag-1.1%, TiO_2/Ag-3.2%, TiO_2/Ag-8.3%, pure TiO_2 nanosponge, P25 and pure TiO_2 powder as photocatalysts under UV-light irradiation. The above results are consistent with those obtained for RhB degradation.

After the reaction, the TiO_2/Ag nanosponge composites are easier separated than the TiO_2 powder or P25 for the recycling applications. The recovered catalysts are washed with water and EtOH, respectively, and then calcined at 450 °C for 2 h. As shown in Figure 9, when the sample TiO_2/Ag-5.1% is used for the reusability test, the photocatalytic activities do not show significant loss up to 5 cycles of RhB photodegradation. The recovered catalysts are analyzed by ICP-AES, which shows that the Ag loading content in TiO_2/Ag nanosponge composites is approximately unchanged. Furthermore, the XPS test of TiO_2/Ag-5.1% sample after photocatalytic reactions is also carried out (refer to the Supporting Information, Figure S1). From Figure S1, it can be seen that the spin energy separation is still 6.0 eV, which indicates that the silver is not oxidized during the reactions. Thus, the above results suggest that TiO_2/Ag nanosponge composites have the excellent stability.

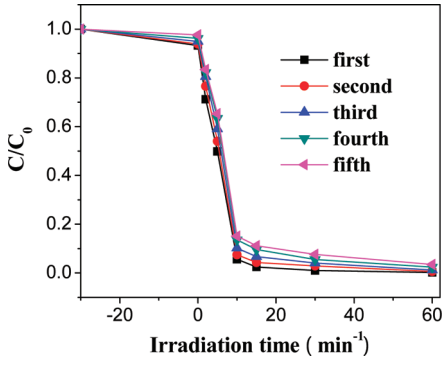

Figure 9. Five cycles of the photocatalytic degradation of RhB using sample TiO_2/Ag-5.1% as the photocatalyst under UV-light irradiation for 60 min.

4. DISCUSSION

According to the above photocatalytic test results, morphology, structure, and physicochemical properties of as-prepared nanosponge materials, we attribute the enhanced UV-light photocatalytic activities of the TiO_2/Ag composites to the following factors. First of all, the enhanced quantum efficiency of TiO_2/Ag composite systems can increase the UV-light photocatalytic activity of the TiO_2/Ag composites. Since the Fermi level of Ag is lower than that of TiO_2, the photogenerated electrons may transfer to the Ag particles deposited on the surface of TiO_2.[30] Then, the transferred electrons are trapped by the metallic Ag due to its strong electron accepting ability, resulting in the effective separation of the electrons and holes. Accordingly, more photoinduced holes and electrons can be produced, which induces more O_2^- species and •OH radicals to participate in RhB or salicylic acid degradation reaction. However, at high Ag loading content (8.3%), the number of active sites capturing the photoinduced electrons is decreased with an increase in the size of Ag particles. Furthermore, the excessive surface Ag particles can also act as the recombination sites, which leads to the decrease in the concentration of photogenerated charge carrier and photocatalytic activities of photocatalysts. Second, the large BET surface areas and mesoporosity of the nanosponge composites will increase the photocatalytic activities of TiO_2/Ag nanosponge materials. The large BET surface areas result in the large contact areas between the active sites and the target substrate. In addition, the mesoporous structure of TiO_2/Ag nanosponges can make the diffusion of the reactants into the mesopores rapidly. Finally, the small size and uniform distribution of the metallic Ag particles on the TiO_2 nanosponges are also responsible for their enhanced photocatalytic activities.

dx.doi.org/10.1021/am3004363 | ACS Appl. Mater. Interfaces 2012, 4, 2781−2787

5. CONCLUSIONS

In this paper, we show that the biological template method is rather flexible to accurately replicate the complex hierarchical morphology of the natural cellulosic substances with metal alkoxides. It is a low-cost and efficient means to produce nanosponge materials with unique structural features. The higher photocatalytic activities of TiO_2/Ag nanosponge composites can be attributed to the following factors which will increase the formation rate of the photoinduced electrons and holes: (1) the high dispersion and small nanoparticle size of Ag nanoparticles, (2) the strong interaction between the metallic Ag particles and TiO_2 samples, and (3) the larger BET surface area and mesoporous structure.

■ ASSOCIATED CONTENT

Supporting Information

Ag 3d XPS spectrum of TiO_2/Ag-5.1% sample after photocatalytic reactions. This material is available free of charge via the Internet at http://pubs.acs.org.

■ AUTHOR INFORMATION

Corresponding Author

*E-mail: yuxd634@nenu.edu.cn; xingyang69cn@yahoo.com.cn.

Notes

The authors declare no competing financial interest.

■ ACKNOWLEDGMENTS

This work was supported by the Fundamental Research Funds for the Central Universities (09QNJJ 014), the National Natural Science Foundation of China (Grant 21073032), the Natural Science Foundation of China (Grant 51102001), and Opening Fund of State Key Laboratory of Inorganic Synthesis and Preparative Chemistry of Jilin University.

■ REFERENCES

(1) Michael, T. *Chem.—Eur. J.* **2007**, *13*, 8376−8388.
(2) Hu, X. L.; Li, G. S.; Yu, J. C. *Langmuir* **2010**, *26*, 3031−3039.
(3) Zhang, L. W.; Wang, Y. J.; Cheng, H. Y.; Yao, W. Q.; Zhu, Y. F. *Adv. Mater.* **2009**, *21*, 1286−1290.
(4) Yadroitsev, I.; Shishkovsky, I.; Bertrand, P.; Smurov, I. *Appl. Surf. Sci.* **2009**, *10*, 5523−5527.
(5) Bayati, M. R.; Golestani-Fard, F.; Moshfegh, A. Z. *Appl. Catal., A* **2010**, *382*, 322−331.
(6) Li, Y. Y.; Ding, Y. *J. Phys. Chem. C* **2010**, *114*, 3175−3179.
(7) Li, Y. X.; Chen, G.; Wang, Q.; Wang, X.; Zhou, A. K.; Shen, Z. Y. *Adv. Funct. Mater.* **2010**, *20*, 3390−3398.
(8) Bouazza, N; Ouzzine, M.; Lillo-Ródenas, M. A.; Eder, D.; Linares-Solano, A. *Appl. Catal., B* **2009**, *92*, 377−383.
(9) Zhang, R.; Wu, H.; Lin, D.; Pan, W. *J. Am. Ceram. Soc.* **2009**, *92*, 2463−2466.
(10) Wang, Q.; Chen, G.; Zhou, C.; Jin, R. C.; Wang, L. *J. Alloys Compd.* **2010**, *503*, 485−489.
(11) Jin, J.; Nishiyama, N.; Egashira, Y.; Ueyama, K. *Microporous Mesoporous Mater.* **2009**, *118*, 218−223.
(12) Kuroda, Y.; Yamauchi, Y.; Kuroda, K. *Chem. Commun.* **2010**, *46*, 1827−1829.
(13) Liu, H. J.; Cui, W. J.; Jin, L. H.; Wang, C. X.; Xia, Y. Y. *J. Mater. Chem.* **2009**, *19*, 3661−3667.
(14) Boissiere, C.; Grosso, D.; Chaumonnot, A.; Nicole, L.; Sanchez, C. *Adv. Mater.* **2011**, *23*, 599−623.
(15) Liu, Z, Y,; Bai, H. W; Sun, D. *Appl. Catal., B* **2011**, *104*, 234−238.
(16) Yeh, T. F.; Syu, J. M.; Cheng, C.; Chang, T. H.; Teng, H. *Adv. Funct. Mater.* **2010**, *20*, 2255−2262.
(17) Klimakow, M.; Klobes, P.; Thunemann, A. F.; Rademann, K.; Emmerling, F. *Chem. Mater.* **2010**, *22*, 5216−5221.
(18) Zhang, P.; Shao, C. L.; Zhang, Z. Y.; Zhang, M. Y.; Mu, J. B.; Guo, Z. C.; Sun, Y. Y.; Liu, Y. C. *J. Mater. Chem.* **2011**, *21*, 17746−17753.
(19) Ahmad, M.; Yingying, S.; Amjad Nisar, A.; Sun, H. Y.; Shen, W. C.; Wei, M.; Zhu, J. *J. Mater. Chem.* **2011**, *21*, 7723−7729.
(20) Miyauchi, M. *Phys. Chem. Chem. Phys.* **2008**, *10*, 6258−6265.
(21) Huang, J. G.; Kunitake, T. *J. Am. Chem. Soc.* **2003**, *125*, 11834−11835.
(22) Klemm, D.; Heublein, B.; Fink, H. -P.; Bohn, A. *Angew. Chem., Int. Ed.* **2005**, *44*, 3358−3393.
(23) Zuruzi, A. S.; MacDonald, N. C.; Moskovits, M.; Kolmakov, A. *Angew. Chem., Int. Ed.* **2007**, *119*, 4376−4379.
(24) Guo, L. L.; Gao, G.; Liu, X. L.; Liu, F. Q. *Mater. Chem. Phys.* **2008**, *111*, 322−325.
(25) Fan, X. X.; Chen, X. Y.; Zhu, S. P.; Li, Z. S. *J. Mol. Catal. A: Chem.* **2008**, *284*, 155−160.
(26) Feng, H. L.; Gao, X. Y.; Zhang, Z. Y.; Ma, J. M. *J. Kor. Phys. Soc.* **2010**, *56*, 1176−1179.
(27) Zhang, Q. J.; Sun, C. H.; Zhao, Y.; Zhou, S. Y.; Hu, X. J.; Chen, P. *Environ. Sci. Technol.* **2010**, *44*, 8270−8275.
(28) Gang, L.; Anderson, B. G.; Grondelle, J.; van Grondelle, J.; van Santen, R. A. *Appl. Catal., B* **2002**, *40*, 101−110.
(29) Yu, J.; Yu, H.; Cheng, B.; Zhou, M.; Zhao, X. *J. Mol. Catal. A: Chem.* **2006**, *253*, 112−118.
(30) Zhang, F.; Pi, Y.; Cui, J.; Yang, Y.; Zhang, X.; Guan, N. *J. Phys. Chem. C* **2007**, *111*, 3756−3761.